AD-A073 835 SOUTHWEST RESEARCH INST SAN ANTONIO TEX F/G 11/6
CRACK TIP PLASTICITY ASSOCIATED WITH CORROSION ASSISTED FATIGUE--ETC(U)
MAY 79 D L DAVIDSON, J LANKFORD N00014-75-C-1038
UNCLASSIFIED SWRI-02-4268 NL

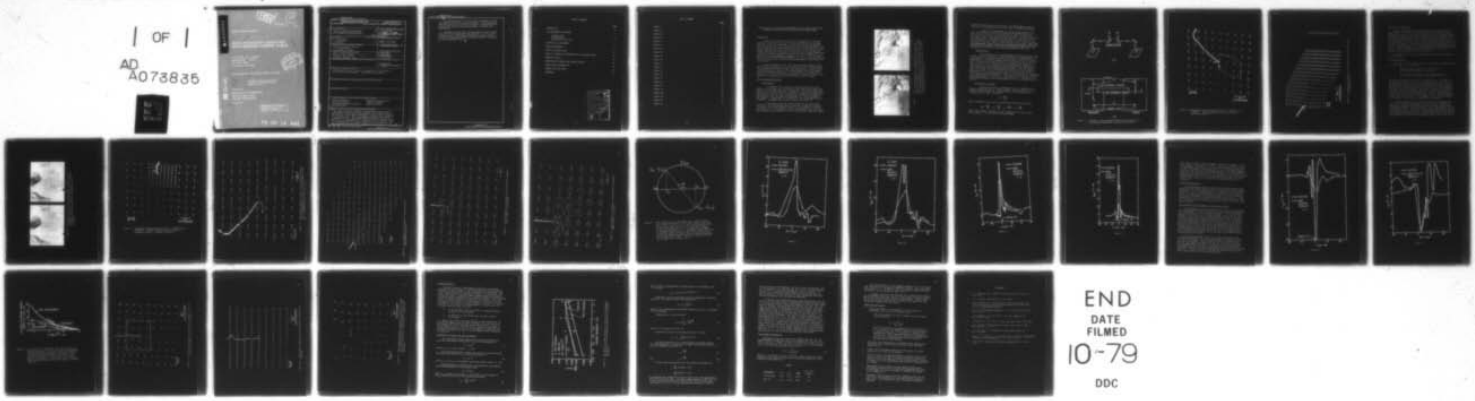

| OF |
AD
A073835

END
DATE
FILMED
10-79
DDC

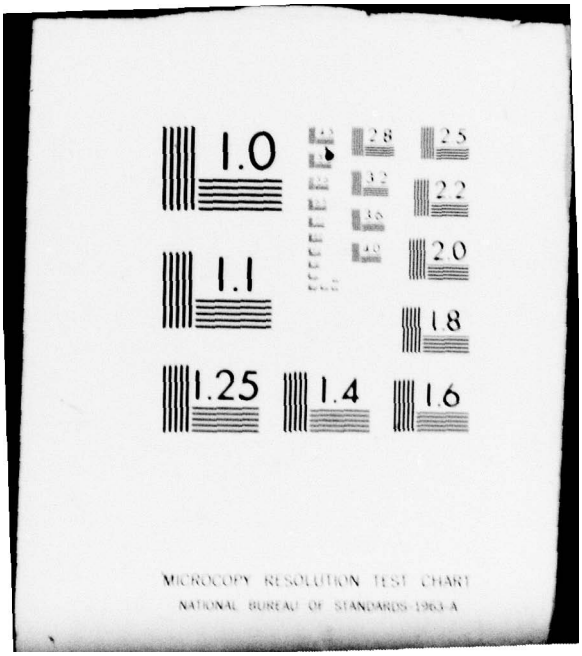
1.0
1.1
1.25
1.4
1.6
2.8
3.2
3.6
4.0
2.5
2.2
2.0
1.8
MICROCOPY RESOLUTION TEST CHART
NATIONAL BUREAU OF STANDARDS-1963-A

CRACK DEVELOPMENT ASSOCIATED WITH CORROSION ASSISTED FATIGUE

N.E. Dowling and J. Landes
Southwest Research Institute
P.O. Drawer 28510
San Antonio, Texas 78284

Interim Report for Period June 1978 - June 1979

Prepared for
OFFICE OF NAVAL RESEARCH
800 North Quincy Street
Arlington, Virginia 22217

UNCLASSIFIED

SECURITY CLASSIFICATION OF THIS PAGE (When Data Entered)

REPORT DOCUMENTATION PAGE

READ INSTRUCTIONS BEFORE COMPLETING FORM

1. REPORT NUMBER

2. GOVT ACCESSION NO.

3. RECIPIENT'S CATALOG NUMBER

4. TITLE (and Subtitle)

CRACK TIP PLASTICITY ASSOCIATED WITH CORROSION ASSISTED FATIGUE

5. TYPE OF REPORT & PERIOD COVERED

Interim Report.
June 1978 - June 1979

6. PERFORMING ORG. REPORT NUMBER

SWRI-02-4268

7. AUTHOR(s)

D. L. Davidson
J. Lankford

8. CONTRACT OR GRANT NUMBER(s)

N00014-75-C-1038

9. PERFORMING ORGANIZATION NAME AND ADDRESS

Southwest Research Institute
P. O. Drawer 28510
San Antonio, TX 78284

10. PROGRAM ELEMENT, PROJECT, TASK AREA & WORK UNIT NUMBERS

NR 036-109/2-25-76(471)

11. CONTROLLING OFFICE NAME AND ADDRESS

Office of Naval Research
800 North Quincy Street
Arlington, Virginia 22217

12. REPORT DATE

31 May 1979

13. NUMBER OF PAGES

367.

31 + prelims

14. MONITORING AGENCY NAME & ADDRESS(if different from Controlling Office)

15. SECURITY CLASS. (of this report)

Unclassified

15a. DECLASSIFICATION/DOWNGRADING SCHEDULE

16. DISTRIBUTION STATEMENT (of this Report)

Reproduction in whole or in part is permitted for any purpose of the United States Government. Distribution is unlimited.

17. DISTRIBUTION STATEMENT (of the abstract entered in Block 20, if different from Report)

18. SUPPLEMENTARY NOTES

19. KEY WORDS (Continue on reverse side if necessary and identify by block number)

Corrosion Fatigue
Crack tip plasticity
Fatigue-environment interaction
Low-carbon steel
Fatigue crack propagation
Crack tip stresses
Crack tip strains

20. ABSTRACT (Continue on reverse side if necessary and identify by block number)

A newly developed technique for measuring in-plane crack tip displacements and strains has been applied to the ongoing study of the effect of a water vapor environment on fatigue crack propagation in low-carbon steel. This stereoimaging technique allows the determination of the in-plane displacements with both high resolution and accuracy at numerous points in the near crack tip region. From these displacements the in-plane elements of the strain tensor and the principal strains and shear strains may be calculated.

DD FORM 1 JAN 73 1473 EDITION OF 1 NOV 65 IS OBSOLETE

UNCLASSIFIED 328 200

SECURITY CLASSIFICATION OF THIS PAGE (When Data Entered)

The principal effect of a water vapor environment on crack tip plasticity is that it causes a decrease in strain magnitude which the material at the crack tip supports, corroborating previous results derived from the measurement of subgrain size distribution.

Information on the effect of environment on crack opening loads and on the "compressive displacements" at the tip of the unloaded crack are also given, as are some preliminary results on the interrelationships between loading frequency, environment and crack propagation rate.

TABLE OF CONTENTS

LIST OF FIGURES

FATIGUE CRACK TIP STRAIN RANGE MEASUREMENTS IN LOW-CARBON STEEL BY THE STEREOIMAGING TECHNIQUE AND THEIR ALTERATION BY WATER VAPOR

Introduction

A number of factors affect the rate of propagation of a fatigue crack at a constant value of cyclic stress intensity, one of the most important of which is environment. Previously, Davidson and Lankford have studied the effect of environment on fatigue crack propagation rates in low-carbon steel by using the propensity of this material to form subgrains; subgrain size may be used as an indicator of the stresses and strains experienced by the material as the crack was passing through, and to measure the energy expended in causing the crack to advance.[1] This report will present preliminary results on the use of a new technique which has been devised for the measurement of strains in the near vicinity of a crack tip and will correlate these measurements with previously reported values.

It must be emphasized that these are preliminary findings which result from the application of a new technique to the questions related to environmentally assisted fatigue crack propagation. One goal of the next several years of effort in this investigation will be to quantify crack tip deformation parameters to the point where it becomes clear whether or not the effects of the environment are surface effects at the crack tip or bulk material effects in the near crack tip region.

The Stereoimaging Technique

Visualization

A method has been devised to measure strains in the near crack tip region which uses the ability of the human visual system (eye-brain) to see in three dimensions (stereopsis). Stereopsis results from the ability of the visual system to compare two images of the same object and, with very high resolution, determine the disparities existing between them.[2] Thus, by comparing photographs of a crack tip taken in two different loading states in a stereoscope, the displacements may be visualized. An example of this effect may be seen in Fig. 1.

Stereopsis exists only along the axis of the eyes; thus, differences in the photographs may be visualized in only one direction at a time. Since cracks generally result in the formation of triaxial strain fields, it is necessary to view the photographs twice, once with the loading direction parallel to the eye axis, and once with the loading

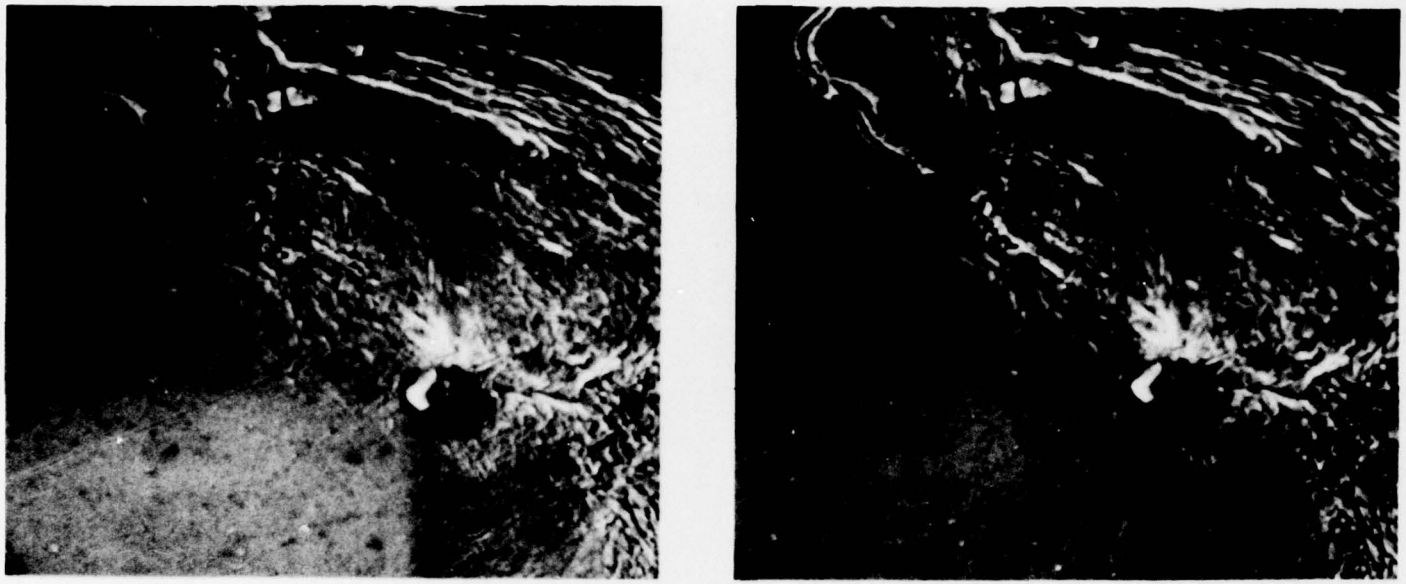

Figure 1. These two photographs are of low-carbon steel, with the fatigue crack grown at $\Delta K = 11$ MN/m$^{3/2}$ in a vacuum of 10^{-5} torr. The photograph on the left (a) was made at K = 2 MN/m$^{3/2}$ and the photograph on the right (b) at K = 13 MN/m$^{3/2}$. By imaging these photographs in a stereoscope, the crack tip displacements may be visualized.

direction perpendicular to the eye axis. The photographs can also be rotated for the determination of the direction of maximum displacement.

When the two photographs are viewed stereoscopically with the crack entering from the top and with the photograph made at the lower load on the left, the following will be seen: the material to the right of the crack will appear lower and that to the left of the crack will appear higher. This means that the material to the right of the crack has moved to the right, and the material to the left of the crack has moved to the left relative to material ahead of the crack. Note that the displacements being visualized are in-plane displacements and not displacements in the z-axis. Since these photographs are made at the same angle of tilt, the out-of-plane displacements cannot be detected.

Quantification

The quantification of displacements which have been visualized is made using the techniques of aerial map making, or photogrammetry. In this procedure, the distance between the same point, as found on the two photographs, is accurately measured using an accurate ruler, or "parallax bar." This may either take the form of a micrometer type scale in the simplest case, or, as is typical for most photogrammetry instruments, a device which accurately measures changes in optical path length as the eyes bring a point into coincidence stereoptically. Thus, the distance apart of any point on the photographs may be measured. By choosing one point ahead of the crack tip, and as far from it as possible, as the reference point, the displacements relative to this point may be determined, as is shown schematically in Fig. 2. This figure also shows the coordinate system established as a reference in reduction of data. Diagrams of the displacements measured from the photographs of Fig. 1 are given in Figs. 3a and 3b.

Calculation of Strains

Engineering strain, or Lagrangian strain, is defined as the change in length per unit of original length. Thus, by passing a curve through the displacement, D_{x_i}, measured in the x_j direction and differentiating that curve, the strain

$$\varepsilon_{ij} = \frac{\partial D_{x_i}}{\partial x_j}$$

may be determined. Thus, the following strain values may be derived:

$$\varepsilon_{xx} = \frac{dD_x}{dx} \quad \varepsilon_{yy} = \frac{dD_y}{dy} \quad \varepsilon_{xy} = \frac{dD_x}{dy} \quad \varepsilon_{yx} = \frac{dD_y}{dx}$$

These strain values, therefore, give the elements of the strain tensor for any point x, y in the field of the photographs.

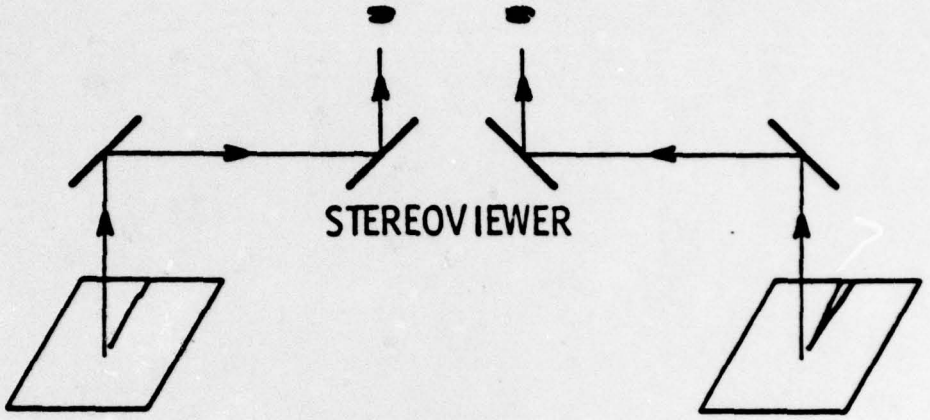

(a)

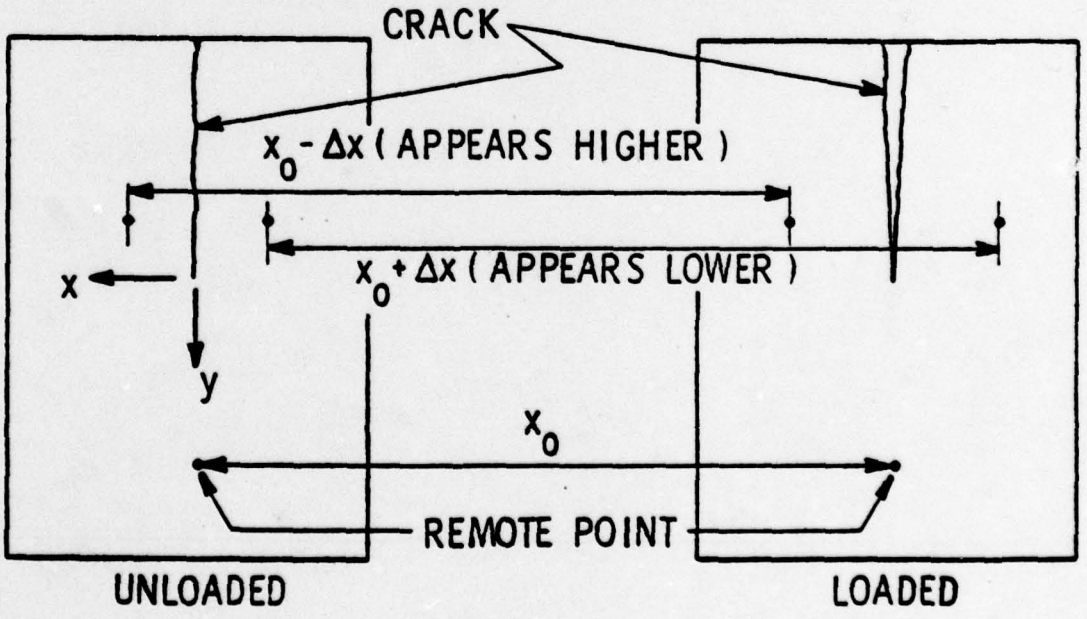

(b)

Figure 2. Schematic of the measurement method used to quantify the stereoimaged displacements visualized from Figure 1.

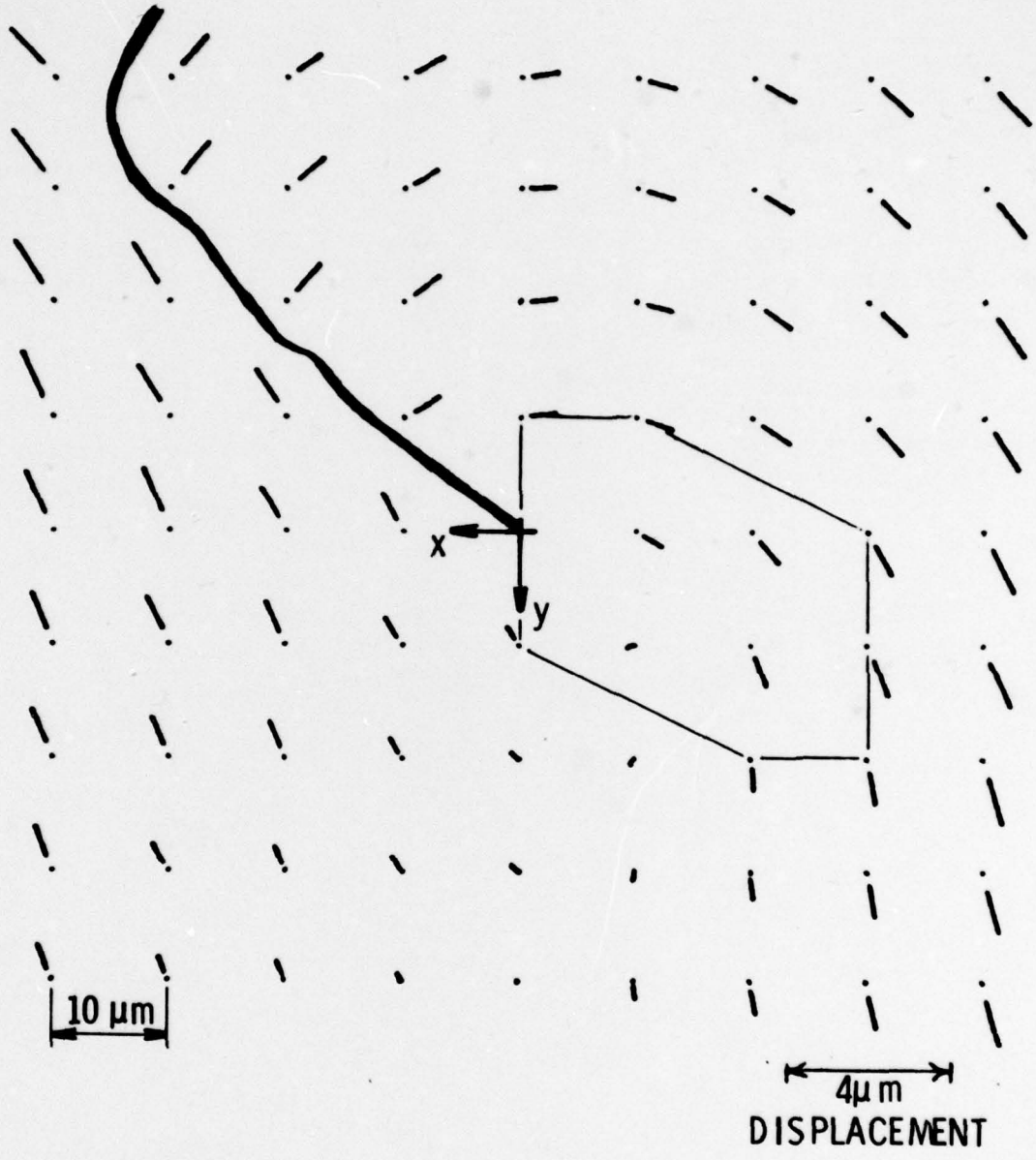

Figure 3a. Displacement diagram upon going from K = 2 $MN/m^{3/2}$ to K = 13 $MN/m^{3/2}$. The area shown is the same as in Fig. 1. Loading was along $\pm$ x.

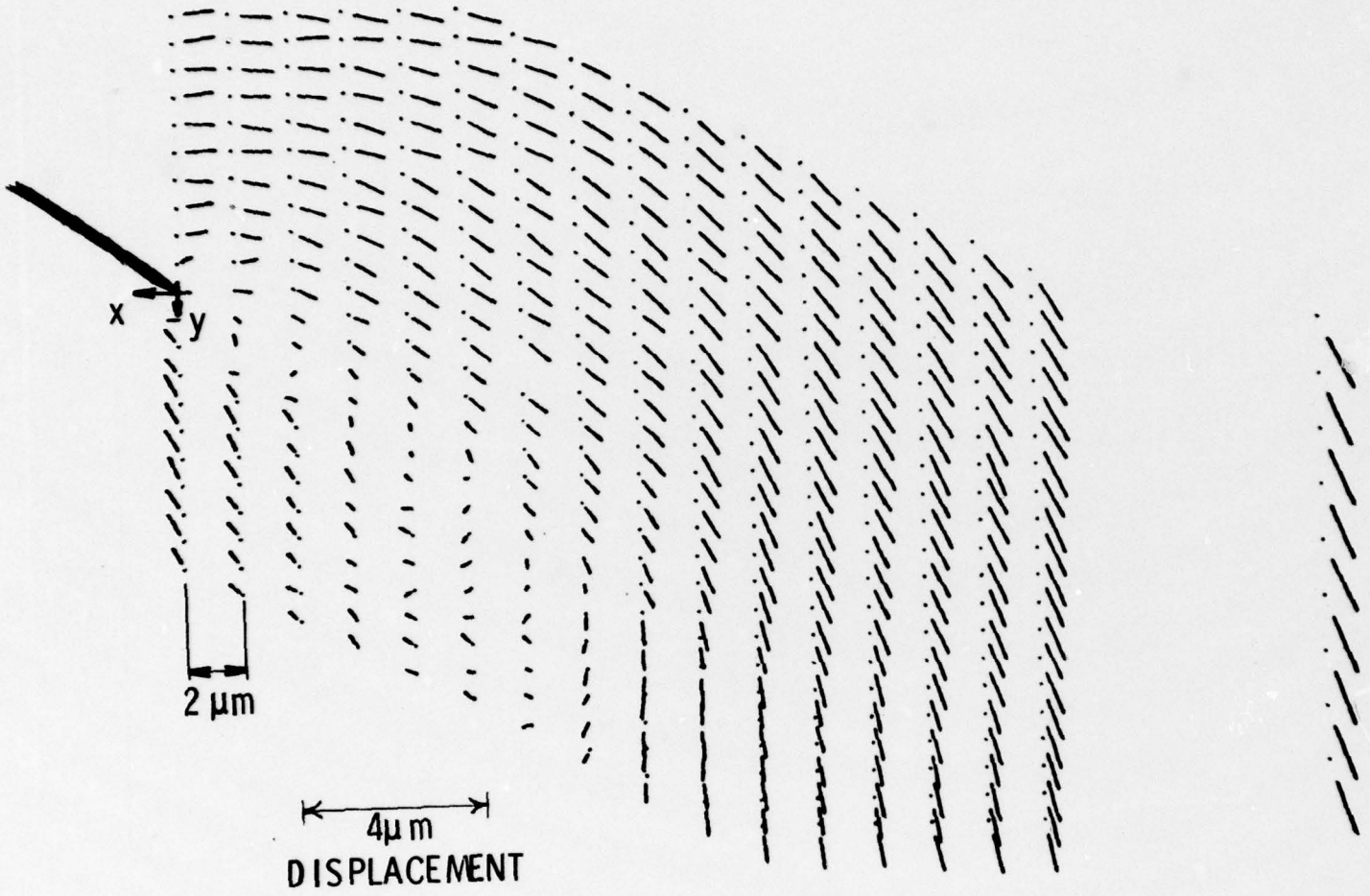

Figure 3b. Displacement diagram for the region very close to the crack tip outlined in (a).

The Effect of Environment

Typical photographs for crack propagation in wet air (100% RH) are shown in Fig. 4; the other conditions are exactly the same as for the photographs of Fig. 1. The crack propagated in a dry environment (vacuum) meanders, and experimentally it has not been possible to obtain a portion of straight crack perpendicular to the loading axis for analysis. It is not yet known whether the analysis of crack tip strains is influenced by the meandering of the crack. For a crack propagated in wet air, meandering is much less prevalent. This characteristic of crack propagation is believed to be inherent in fatigue crack propagation for this material in the $8 < \Delta K < 12$ MN/m$^{3/2}$ range, $R = 0.05$, but this point is still under investigation. Some preliminary observations indicate that the amount of meandering may be dependent on loading frequency.

The displacement map for crack propagation in the wet environment is shown in Fig. 5.

Strain Measurements

In order to compute strains from the displacement measurements shown in Figs. 3 and 5, it is necessary to

1) smooth the displacement data to compensate for photogrammetric measurement inaccuracies

2) fit curves to the resulting data, taking the slope at the coordinate of interest to obtain the strain.

The details of how this is done may be found in Ref. 3. In addition to the normal strains ε_{xx} and ε_{yy}, and the shear strain $\gamma_{xy} = \varepsilon_{xy} + \varepsilon_{yx}$, the maximum principal strain ε_{11}, the minimum principal strain ε_{22}, and maximum shear strain γ_{max}, and their directions, may also be computed. Figures 6 and 7 present the Mohr's strain circles for cracks propagated in the wet and dry environments, respectively. Although these figures are complex, all the information which can be derived at each point is found in each Mohr's circle representation. Figure 8 explains how to read the Mohr's circle information in Figs. 6 and 7. Since the diameter of the circle at each point is a measurement of γ_{max}, the distribution of this quantity can be directly assessed from the figures.

Detailed comparisons of the normal strains and the maximum shear strain as a function of environment are given in Figs. 9 through 14. These figures present normal strain data in a form more readily assimilable than the Mohr's circles, and allow a direct demonstration of the environmental effect. The maximum normal strain in the loading direction is lowered from nearly 12% to 6% by the environment (Fig. 9), and Fig. 10 shows a similar reduction for γ_{max}. Figures 11 and 12 show that ε_{xx} and γ_{max} decrease very rapidly with increasing distance ahead of the crack

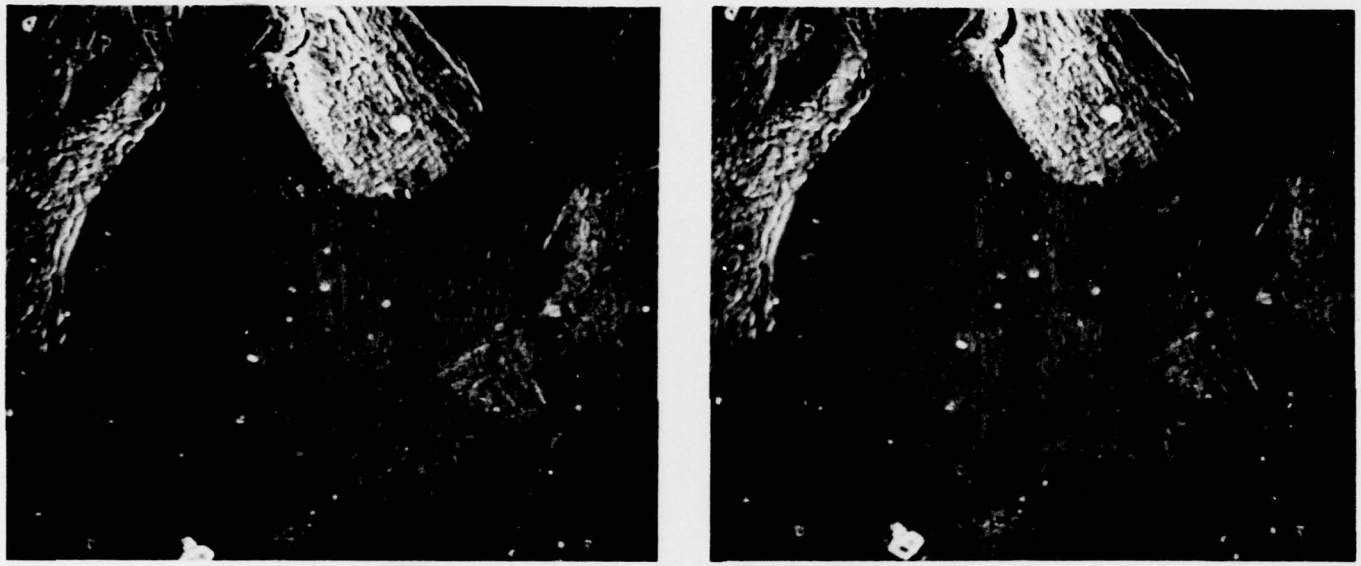

Figure 4. Photographs of the crack tip for growth in 100% relative humidity. Left (a) K = 2 $MN/m^{3/2}$, right (b) K = 13 $MN/m^{3/2}$. By imaging these photographs the displacements may be visualized.

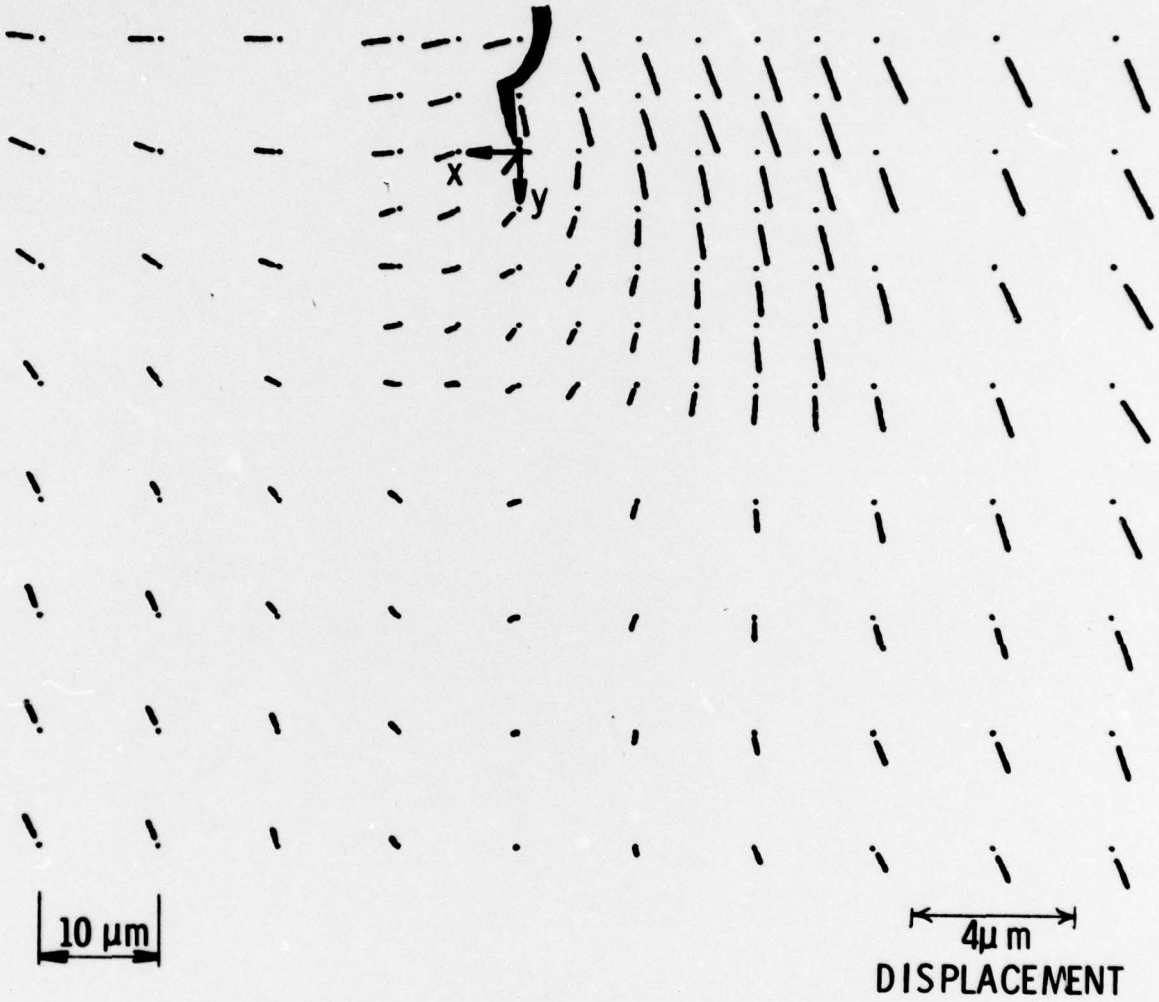

Figure 5. Displacement diagram upon going from K = 2 $MN/m^{3/2}$ to K = 13 $MN/m^{3/2}$. The area shown is the same as in Fig. 4. Loading was along $\pm$ x. Compare with Fig. 3a.

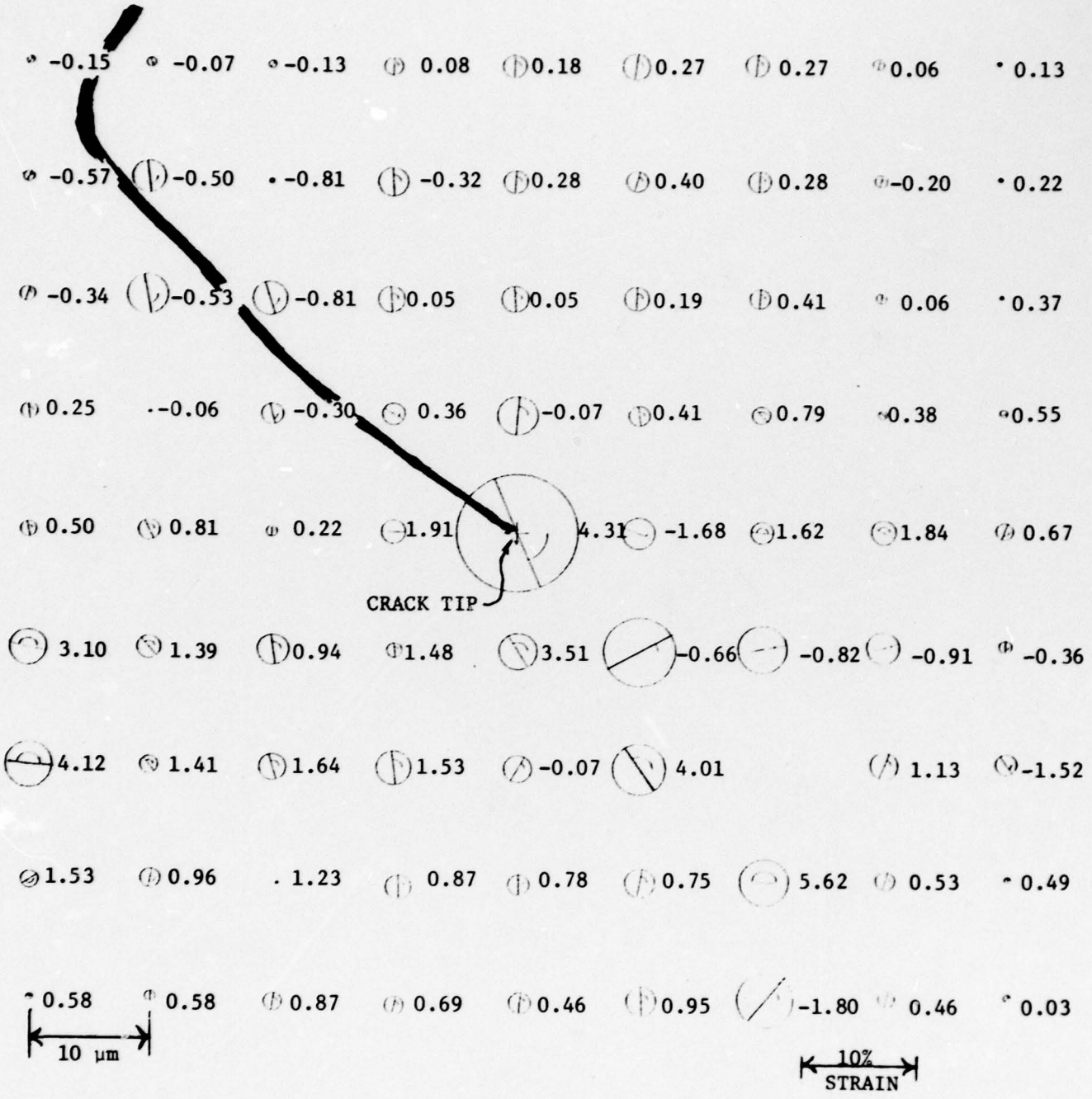

Figure 6a. Strain diagram (Mohr's circles), dry environment, derived from the displacements in Fig. 3a. Circle diameter is the γ_{max}. The number given at each point is ε_m.

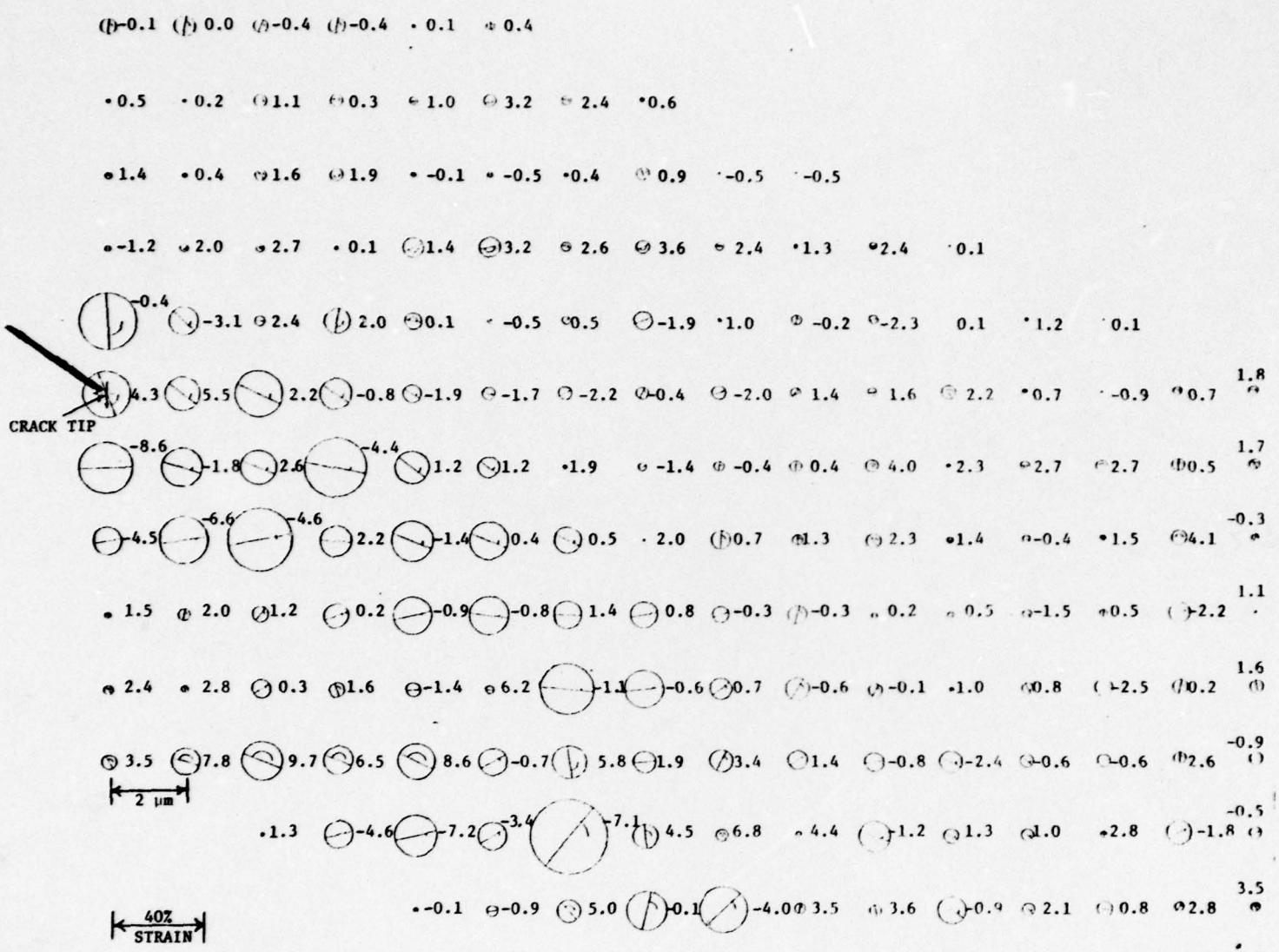

Figure 6b. Strain diagram, dry environment, derived from the displacements in Fig. 3b.

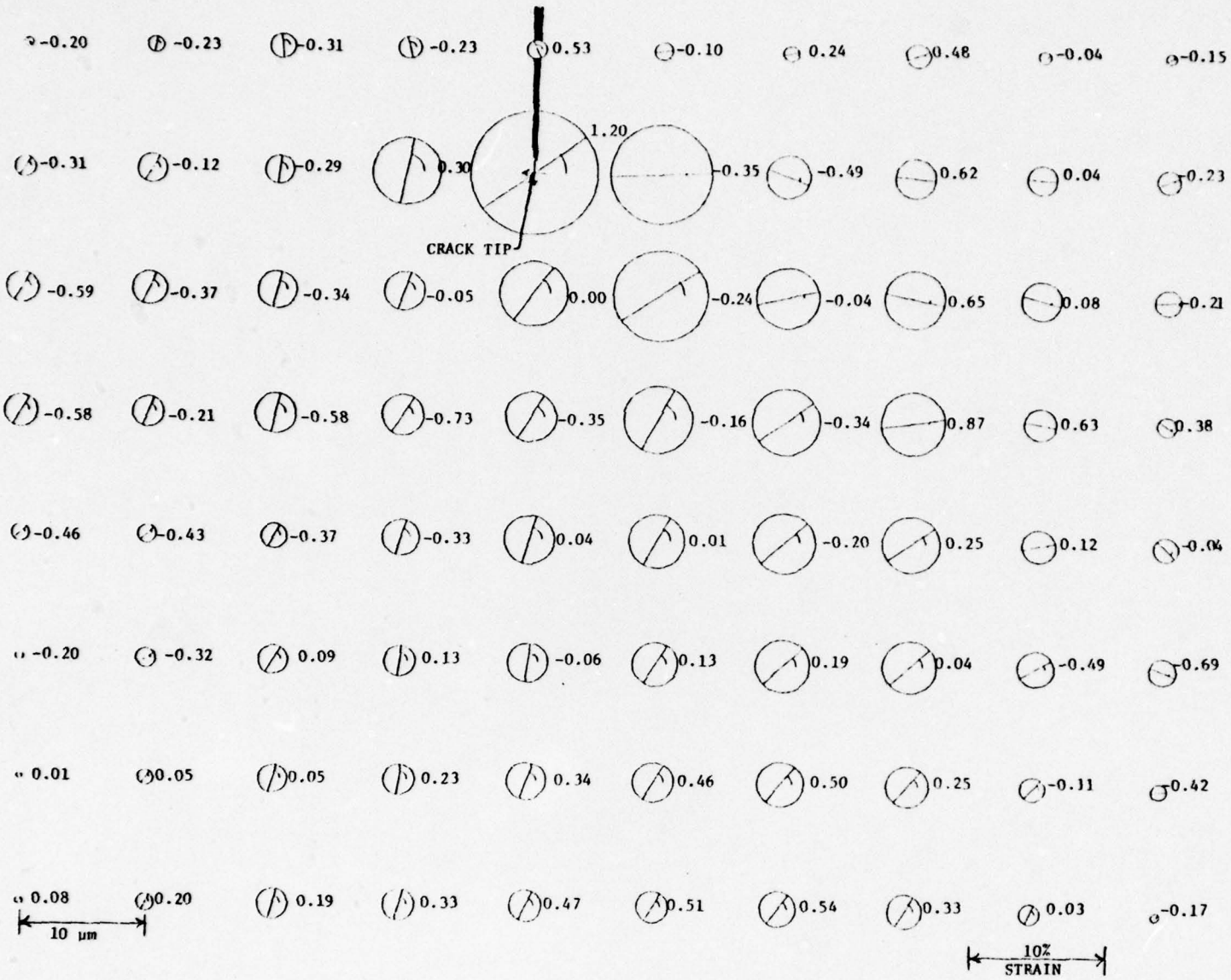

Figure 7a. Strain diagram, wet environment, derived from the displacements in Fig. 5, coarse grid.

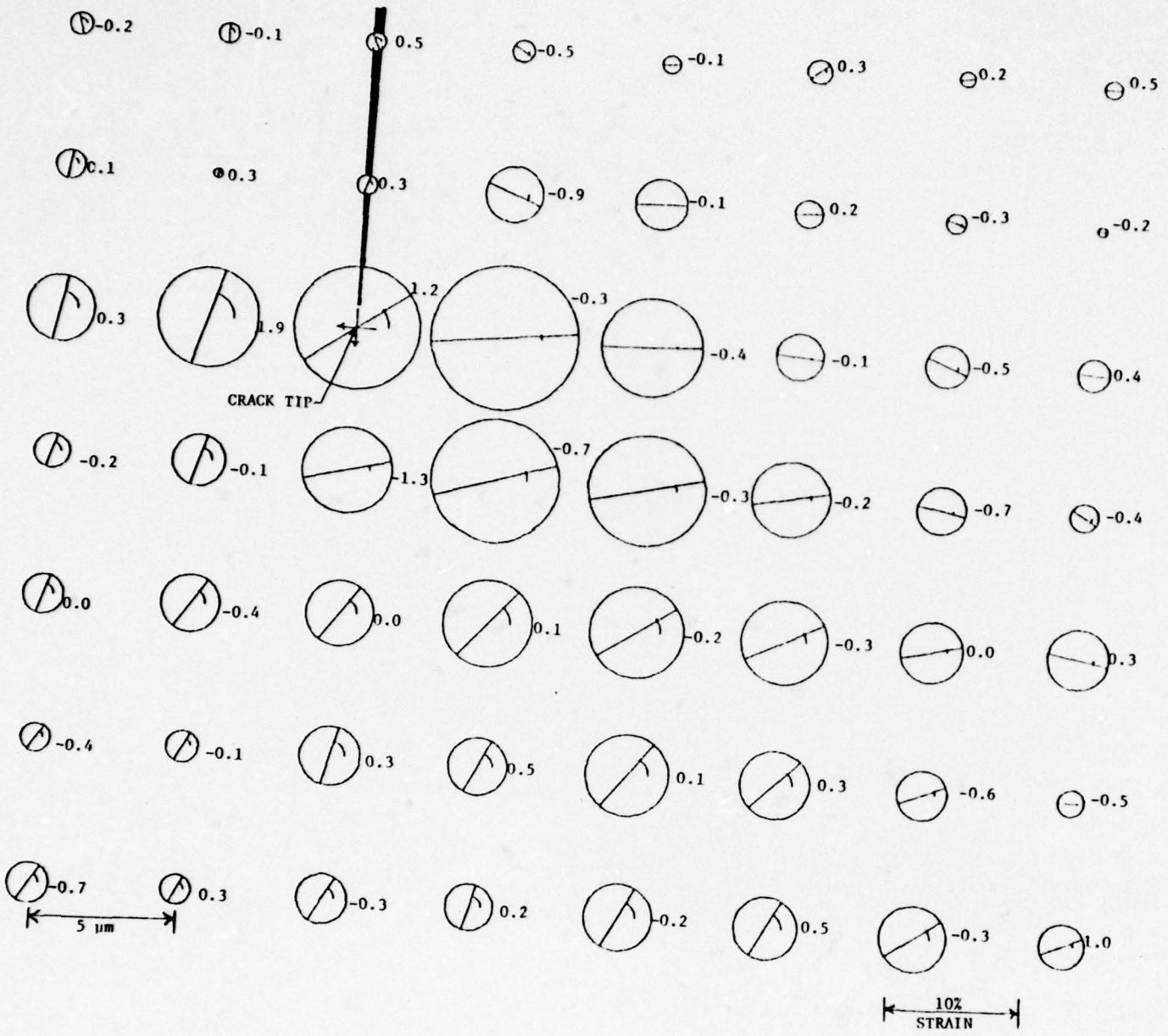

Figure 7b. Strain diagram, wet environment, derived from the displacements in Fig. 5, fine grid.

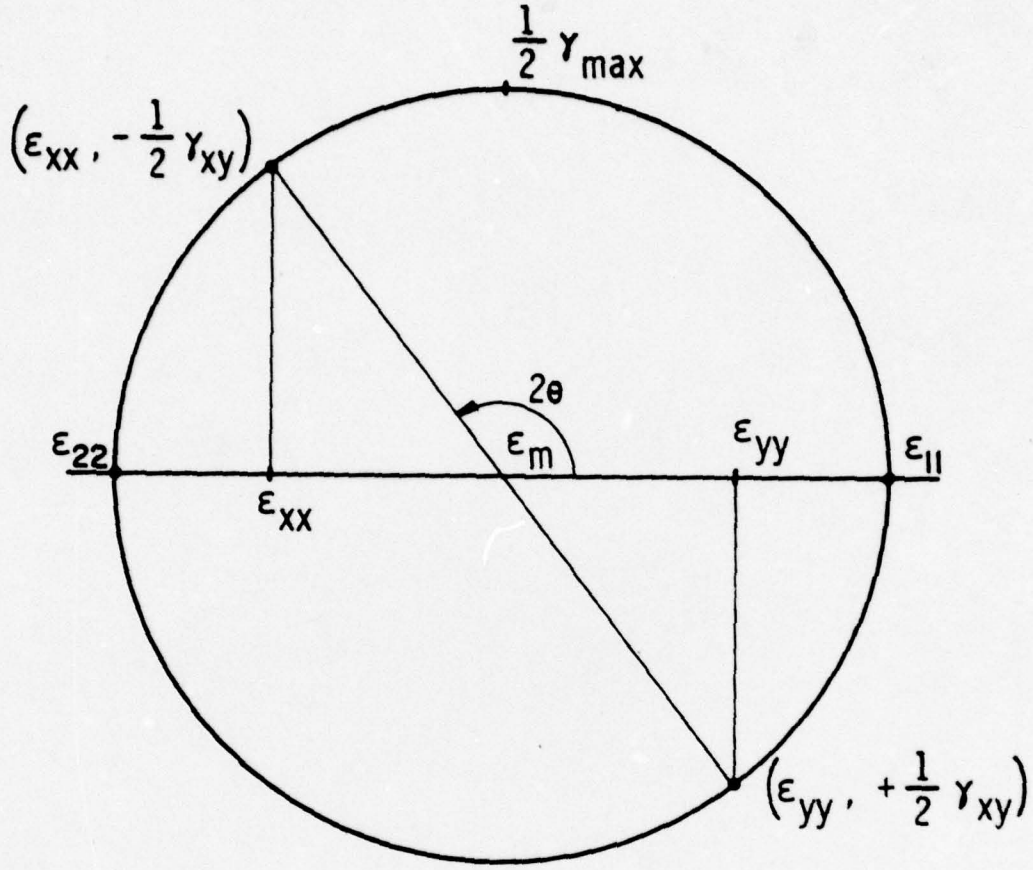

Figure 8. Mohr's strain circle. The points $(\varepsilon_{xx}, -\gamma_{xy}/2)$ and $(\varepsilon_{yy}, \gamma_{xy}/2)$ define the diameter of the circle, and its center is at $\varepsilon_m = (\varepsilon_{xx} + \varepsilon_{yy})/2$, $\gamma_{xy} = 0$. The circle intercepts along the horizontal axis ($\gamma_{xy} = 0$), are the principal strains, ε_{11} and ε_{22}, along which $\gamma = 0$. The angle 2θ corresponds to the angle θ between the x, y coordinates and the directions of principal strain. On Figs. 6 and 7, 2θ is shown as the arc from the maximum principal strain (the undrawn horizontal axis) to the x-axis (drawn). See Refs. 3 and 4 for more detail on Mohr's circle construction.

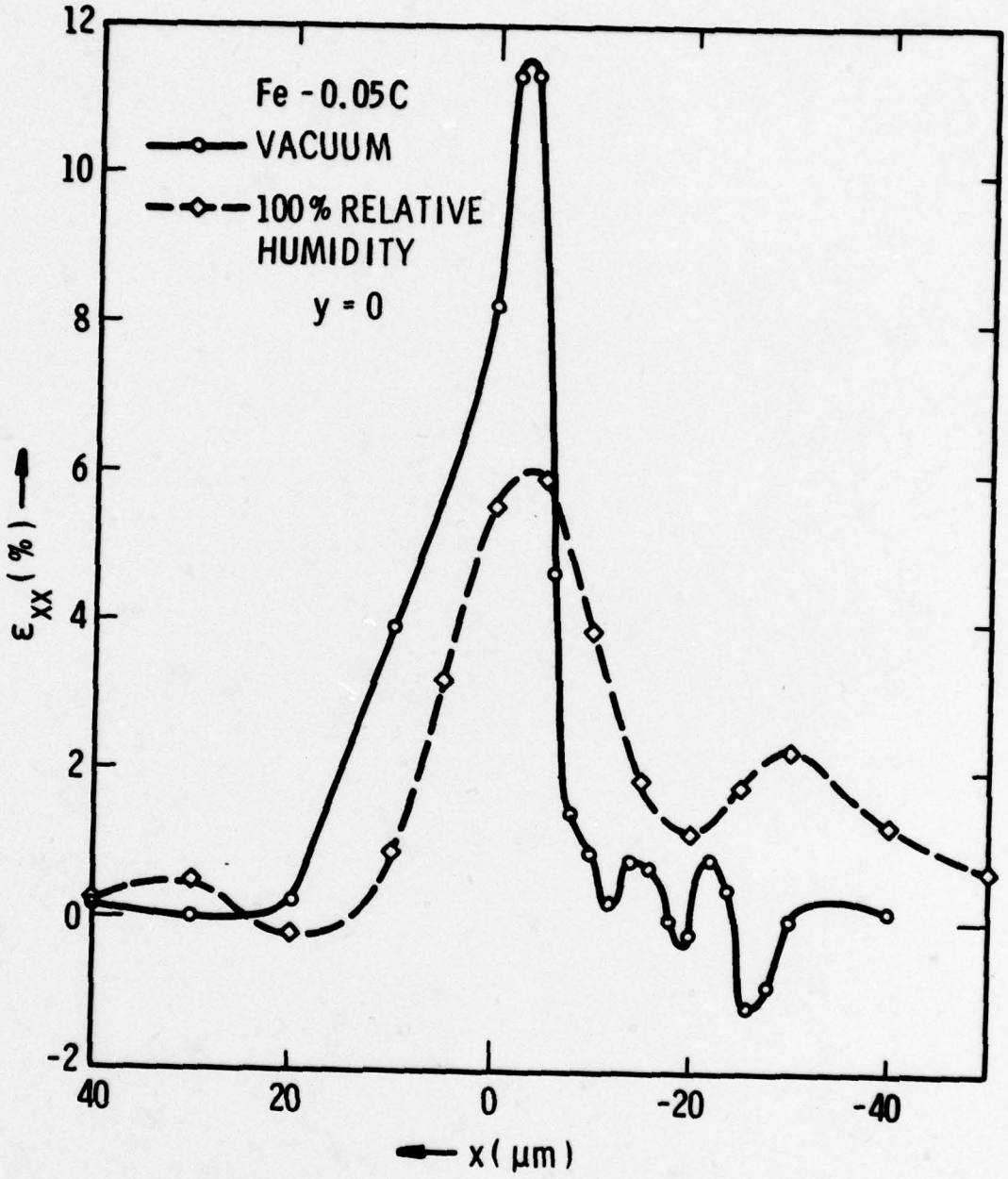
Fe - 0.05C
VACUUM
100% RELATIVE HUMIDITY
y = 0
12
10
8
6
4
2
0
-2
ε_{xx} (%)
40
20
0
-20
-40
x (μm)

Figure 9.

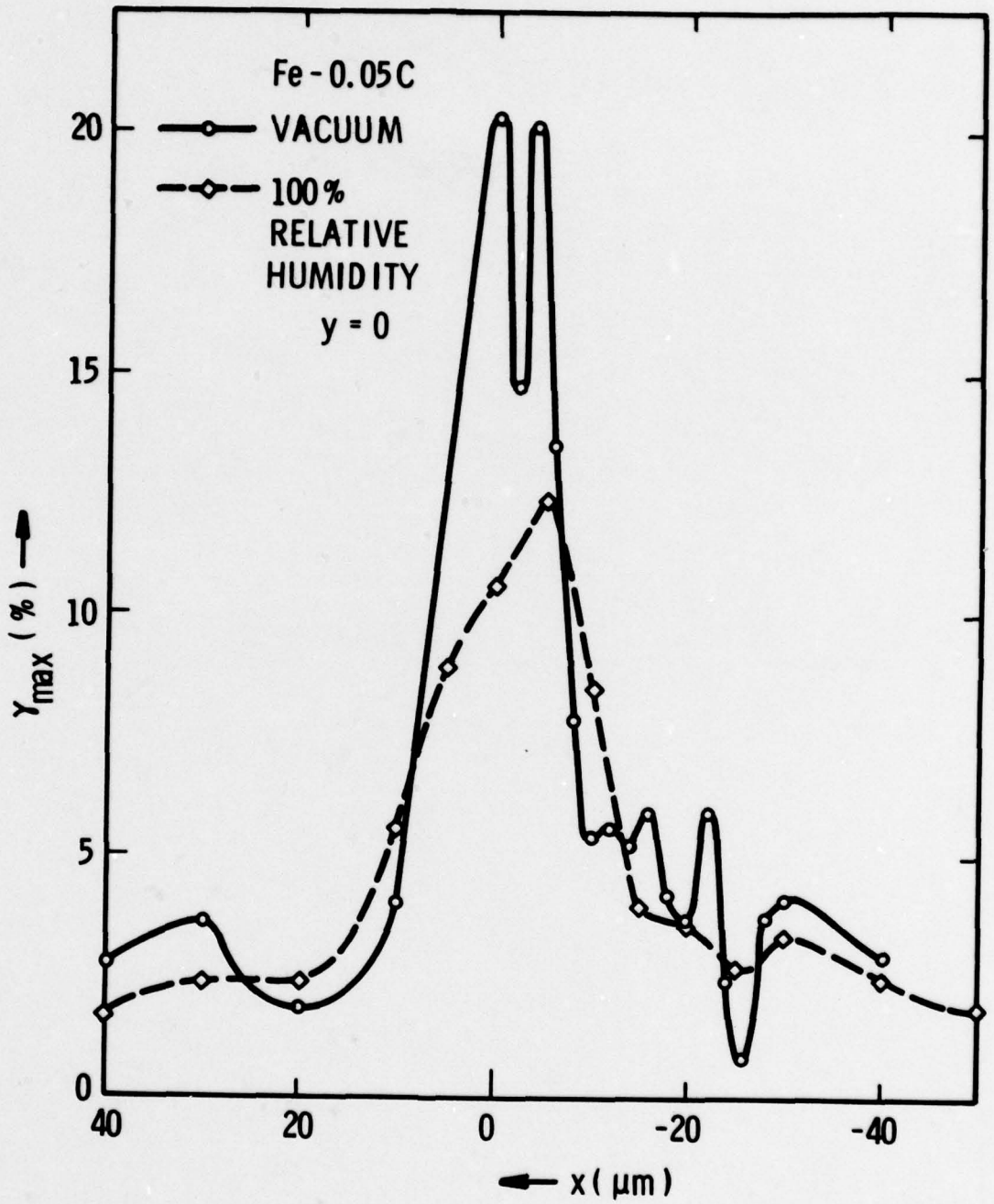
Fe - 0.05C
VACUUM
100% RELATIVE HUMIDITY
y = 0
20
15
10
5
0
γ_{max} (%)
40
20
0
-20
-40
x (μm)

Figure 10.

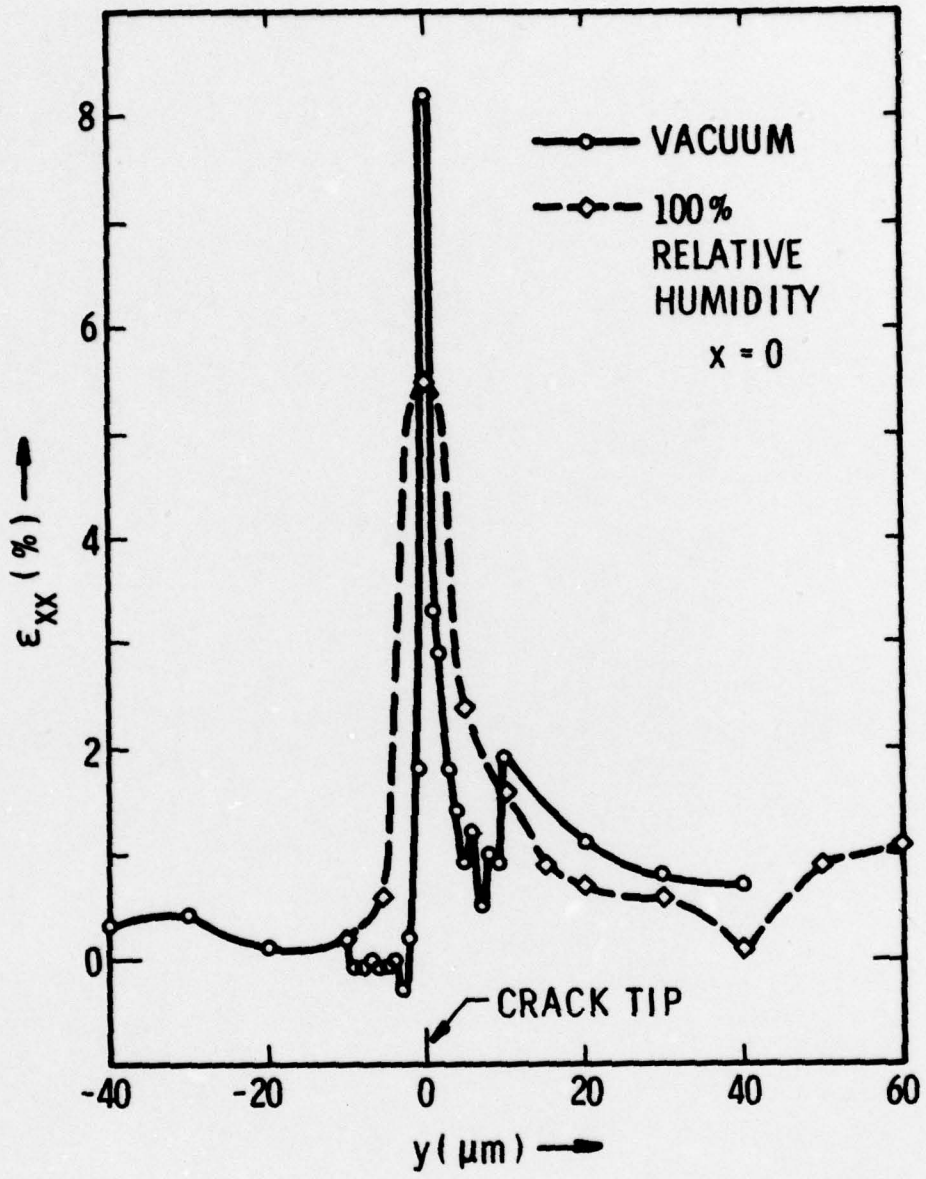
VACUUM
100% RELATIVE HUMIDITY
x = 0
CRACK TIP
ε_{xx} (%)
y (μm)
8
6
4
2
0
-40
-20
0
20
40
60

Figure 11.

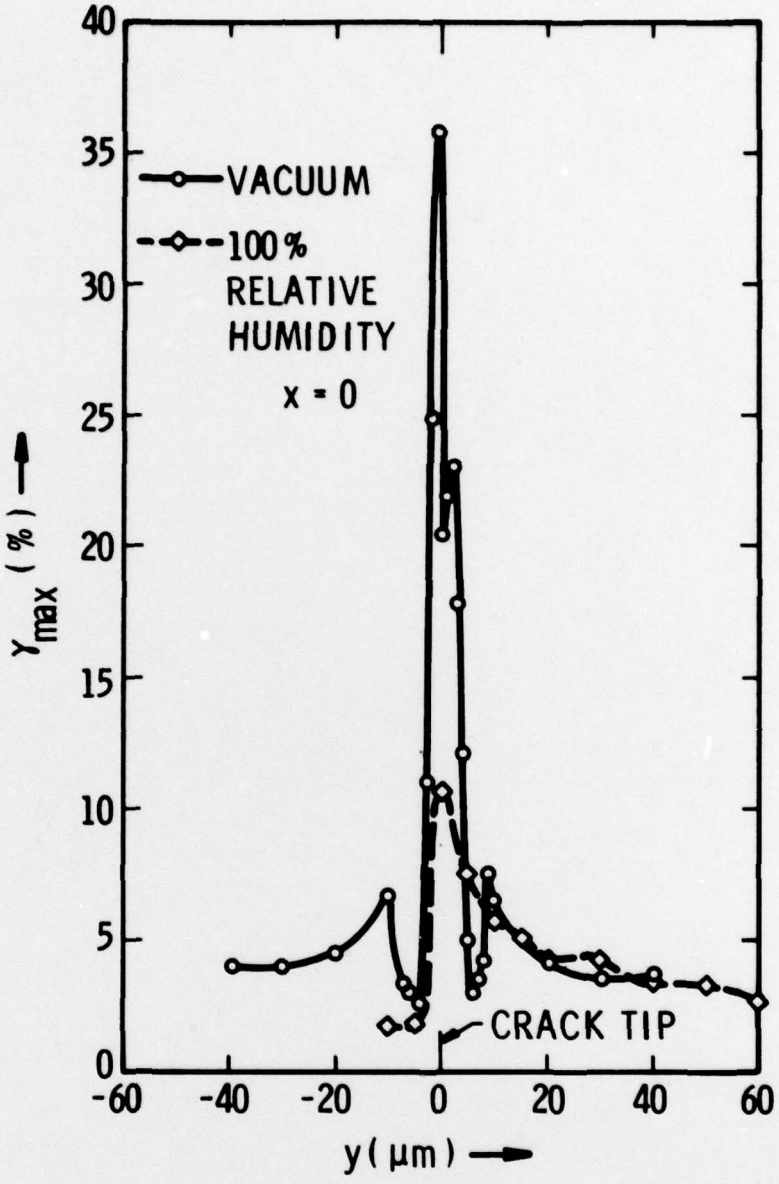
VACUUM
100%
RELATIVE
HUMIDITY
x = 0
CRACK TIP
γ_{max} (%)
y(μm)
40
35
30
25
20
15
10
5
0
-60
-40
-20
0
20
40
60

Figure 12.

tip. Figure 13 shows a rather remarkable difference in behavior of the normal strain in the plane of the crack, ε_{yy}, due to environment. There is considerable oscillation for the crack tip excluding water vapor, but for both environments, the maximum value of ε_{yy} occurs slightly ahead of the actual crack tip, with the maximum magnitude for the dry environment being about four times that for the wet environment. The decrease in ε_{yy} along the loading direction also occurs rapidly, and is not much affected by environment, Fig. 14. It is not presently known whether the oscillations in the -x direction for the dry environment strains are of consequence.

Crack Tip Opening Loads

The stereoimaging technique, together with the SEM loading stage, allows the relationship between crack tip opening and load to be readily determined. For a crack propagated at $\Delta K = 8$ MN/m$^{3/2}$, at a loading frequency of 0.03 Hz, the distance behind the crack tip where the crack is open vs. the applied stress intensity is shown in Fig. 15 for both the wet and dry environments. The main difference is that there is a large hysteresis for the dry environment and virtually none for the wet. Note that for neither case is the crack open to the crack tip until full load has been applied.

Crack Tip Material Displacements for the Unloaded Crack

By photographing the specimen ahead of the fatigue crack and again after propagating the crack into that region, the material displacements due to the presence of the crack may be examined. It is by this comparison that the concept of a "clamping stress" on the crack tip may be examined. Such an experiment has been performed for both the wet and dry environments, and the displacements have been measured. Diagrams of these displacements are shown in Figs. 16 and 17. For both environments, the displacements which result from the presence of the crack have been in the opposite direction to the displacements which result when the crack is loaded; thus, these displacements are indicative of a "clamping strain" in the crack tip region. We are exercising caution in the interpretation of these results because of the possibility of some other logical explanation, but at this time, the "clamping strain" concept appears to be valid.

As was predicted might be the case in last year's report, the "clamping displacements" for the wet environment are smaller than those for the dry environment. This information appears to correlate well with the crack opening information in Fig. 15. Derivation of strains from the displacement data has not yet been done, but the strains will be considerably larger for the dry environment case than for the wet environment because of the larger displacement gradients which are evident in Fig. 16. Further derivation of information from these results must await detailed analysis of the displacement data.

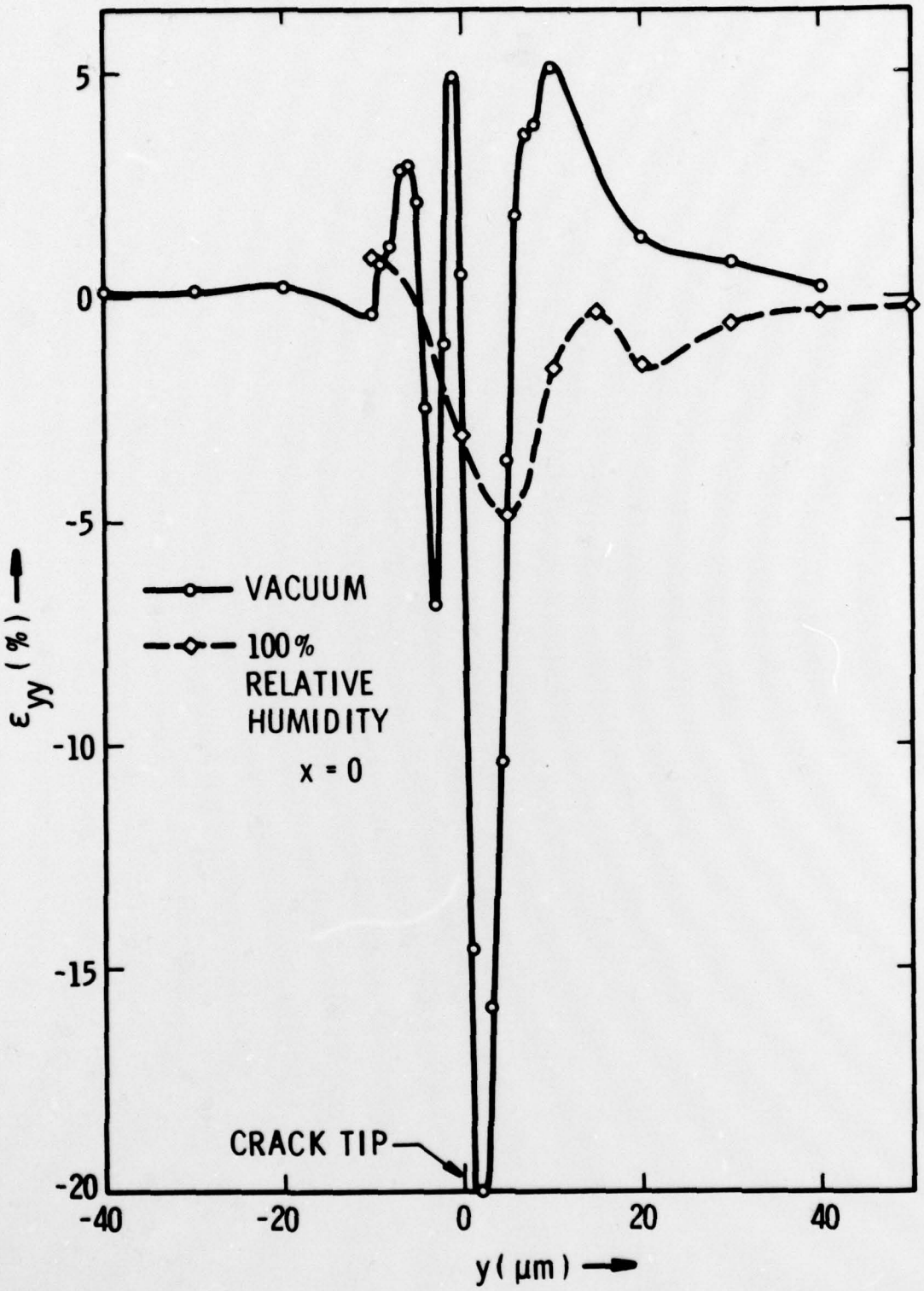
5
0
-5
-10
-15
-20
-40
-20
0
20
40
ε_{yy} (%)
y (μm)
VACUUM
100% RELATIVE HUMIDITY
x = 0
CRACK TIP

Figure 13.

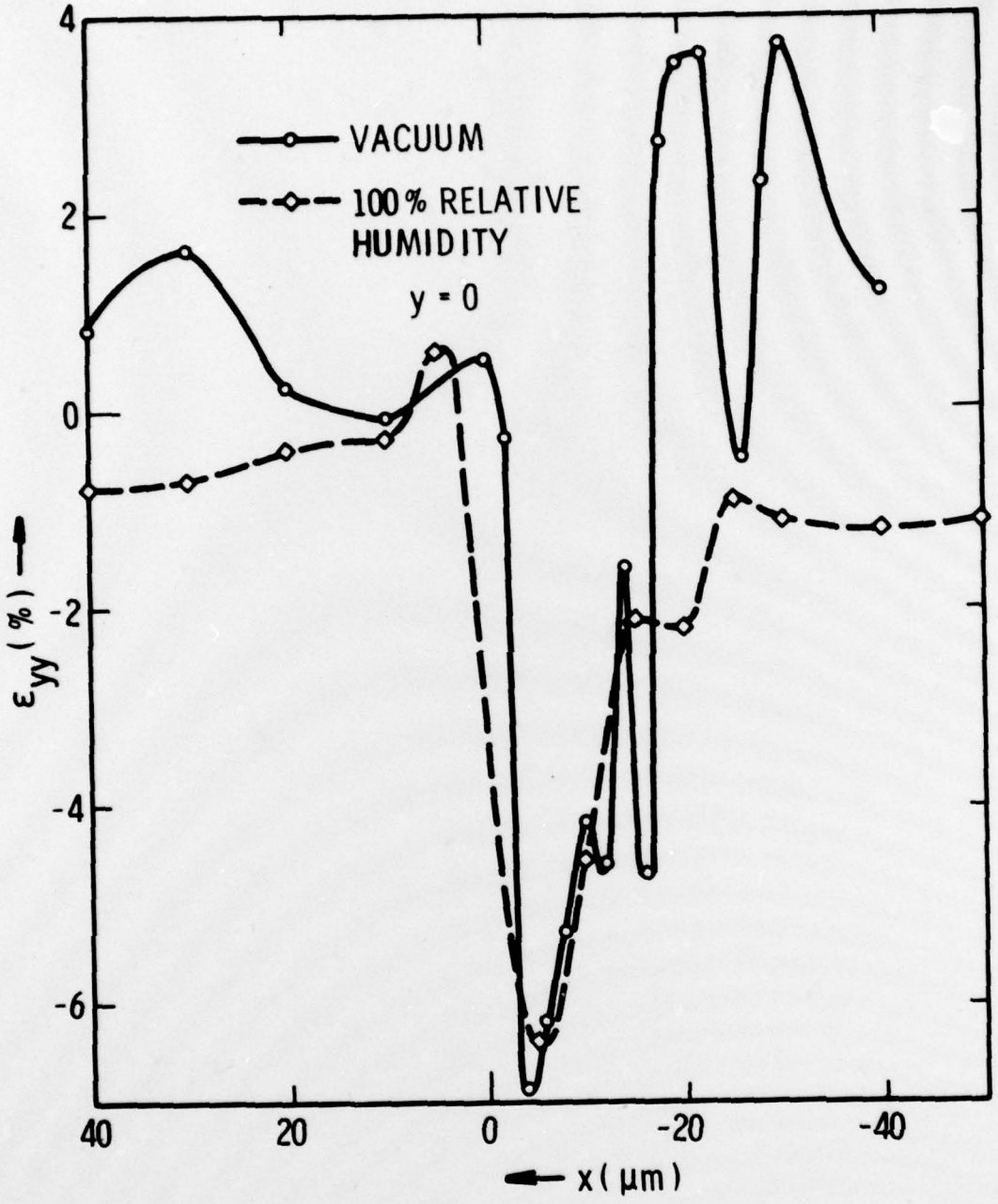
VACUUM
100% RELATIVE HUMIDITY
y = 0
4
2
0
-2
-4
-6
ε_{yy} (%)
40
20
0
-20
-40
x (μm)

Figure 14.

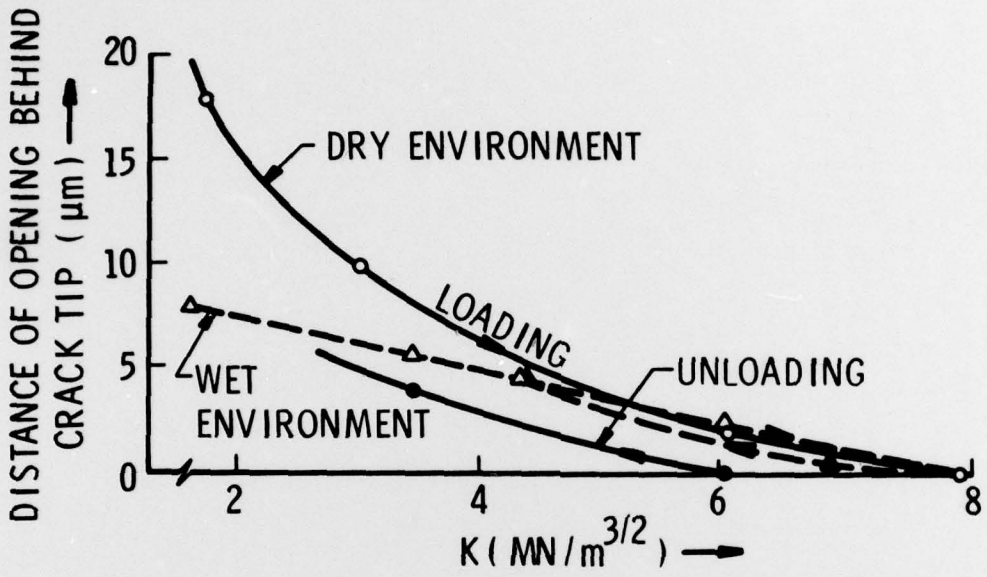

FIGURE 15. The distance in μm behind the crack tip for which the crack is open vs K for both dry and 100% RH environments. Although actual data is plotted, a sufficient number of crack tips have been examined for this behavior to be considered as "typical." This figure is for cracks grown at a frequency of 0.03 Hz, and there is evidence that the behavior shown is altered by changes in loading frequency.

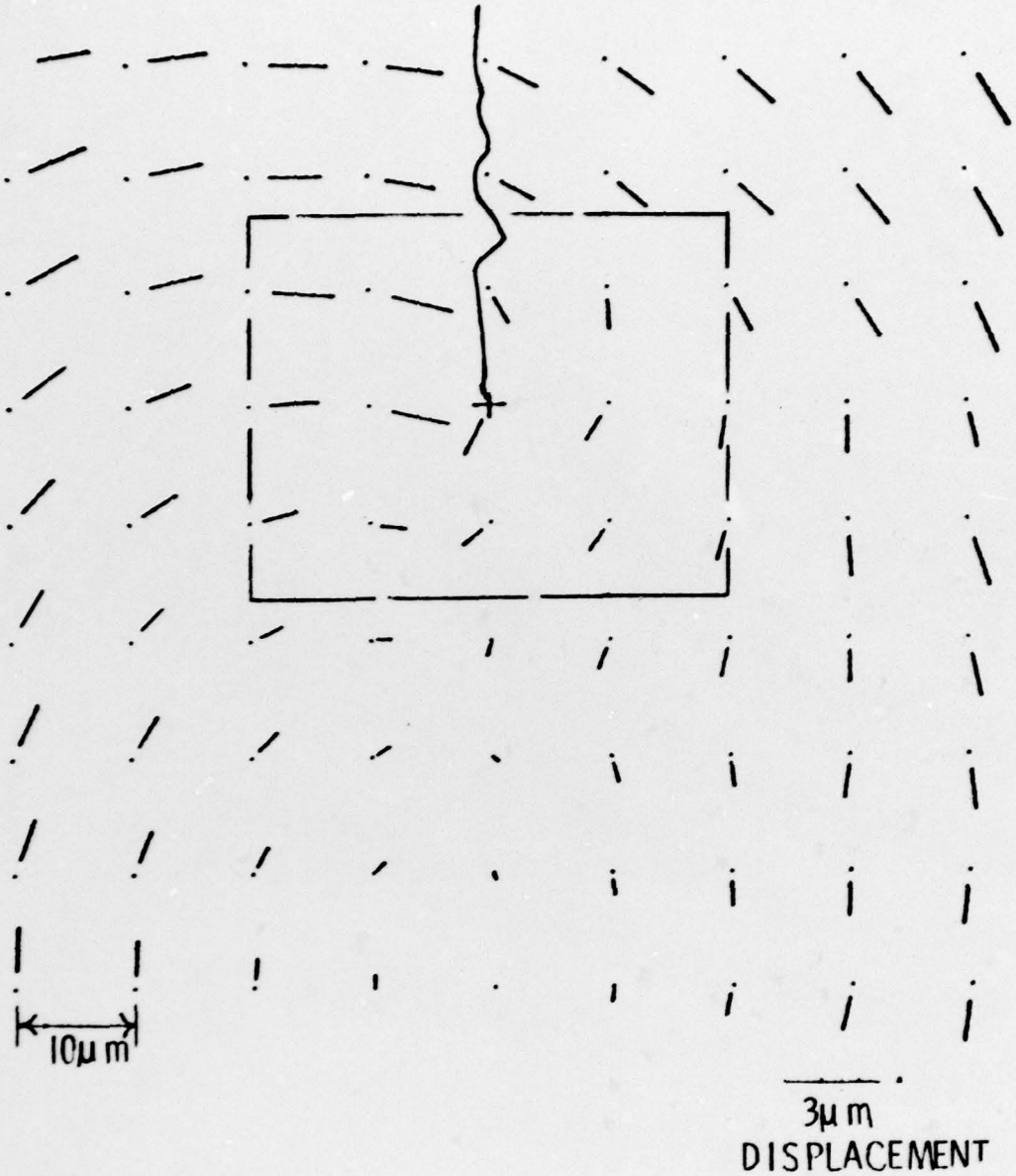

Figure 16a. Displacement diagram for uncracked vs unloaded crack, dry nitrogen environment, 0.03 Hz loading frequency.

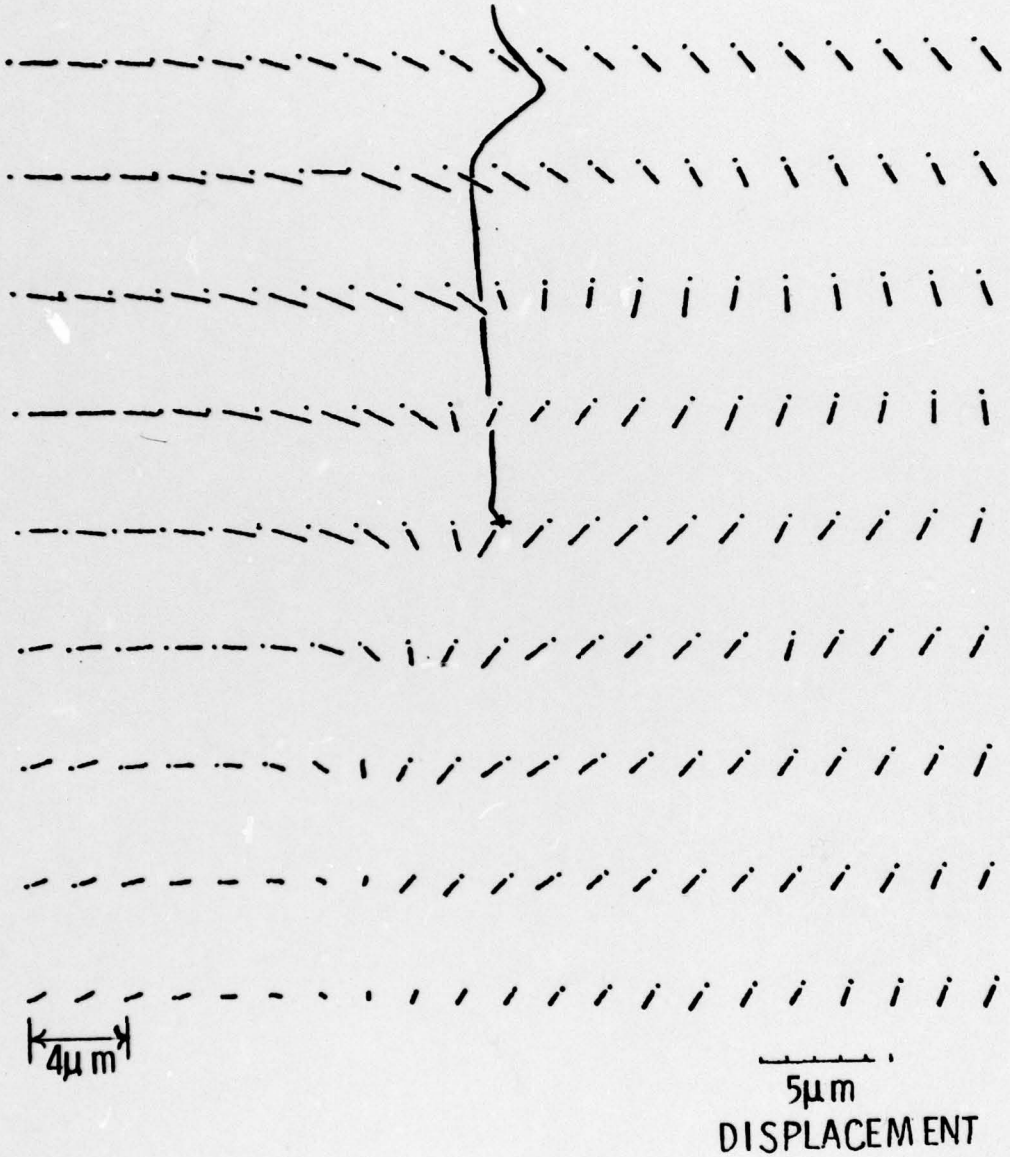

Figure 16b. Displacement diagram within the rectangular area shown in Fig. 16a.

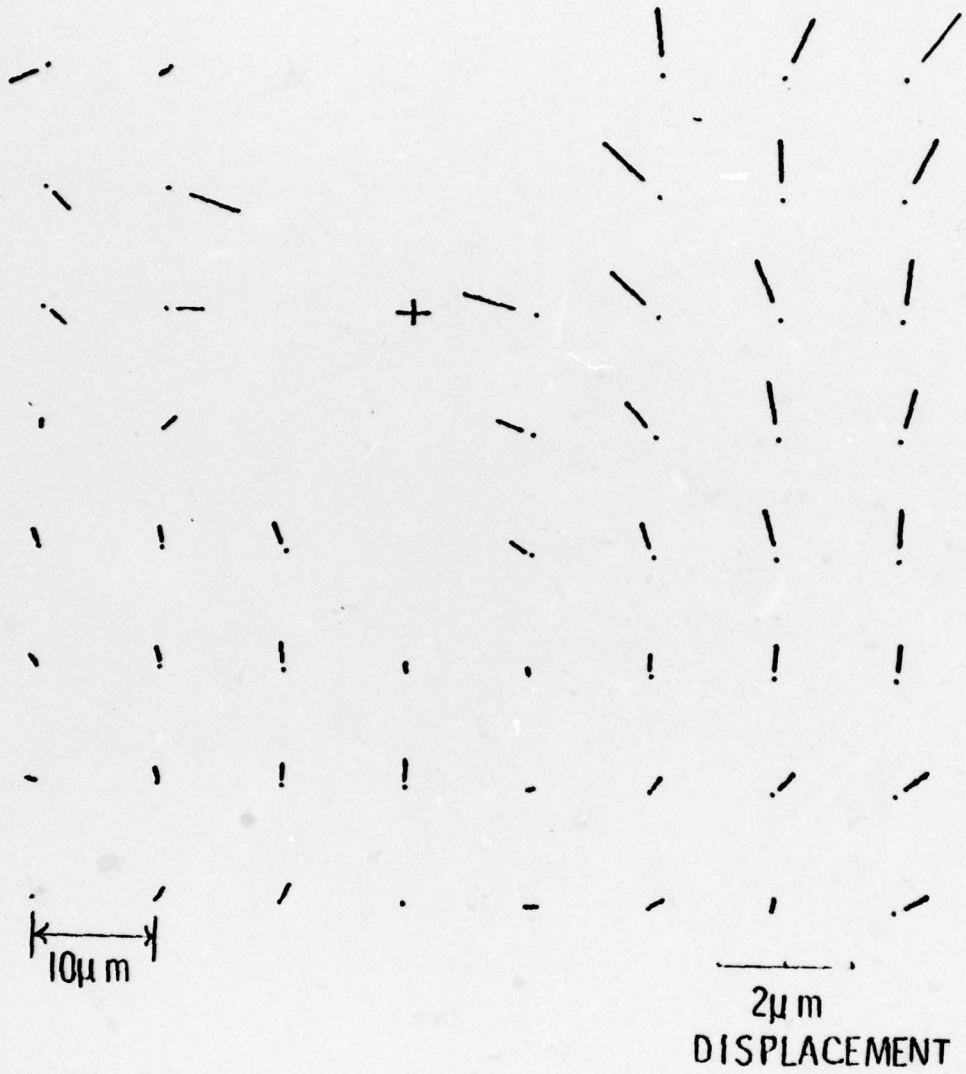

Figure 17. Displacement diagram for uncracked vs unloaded crack, wet air environment, 0.03 Hz loading frequency. Note: some points are missing due to difficulties in imaging the photograph.

Frequency Effects

Because the effect of environment is expected to be exposure dependent,[5] both frequency of load application and relative humidity, or partial pressure of water vapor, are expected to be important. But because body-centered cubic materials are known to be strain-rate sensitive, there may be a coupling between loading frequency and material properties, which are dependent on the thermal activation of dislocations, as well as between frequency and exposure to environment. Thus, some results are being obtained for crack propagation in both wet and dry environments as a function of loading frequency. The effect of loading frequency on crack growth in both environments is shown in Fig. 18. From these data two points are clear:

1) In dry nitrogen, there is an effect of loading frequency on the rate of crack growth.

2) In 100% RH, the crack growth rate is greater than in dry nitrogen.

What is not clear is the exact amounts of these results for the 100% RH environment; thus, two lines are shown: the solid line is a least squares fit for all the data, and the dotted line is a best fit for the data below 1 Hz. Further work on this point is necessary to better quantify these effects, but it does appear as though care must be taken to determine just what is an environmental effect and what is a rate effect.

Correlation of Present and Previous Results

The relationship between subgrain size and energy expended per cycle was established and presented in the 1977 Interim Report as

$$W_c = W_{co} d^{-m} \tag{1}$$

where $W_{co} = 3 \pm 1$ J/m^2, d(μm), $m = 1 \pm 0.1$.

The relationship between subgrain size and cyclic stress range was established and presented in the 1978 Interim Report as

$$\Delta\sigma = C_1 d^{-n} \tag{2}$$

where $C_1 = 2.25\ \sigma_y$, $\sigma_y = 218$ MN/m$^{3/2}$ (the yield stress), d(μm), n = .262.

Combining these two relations with a calculation of the energy per cycle from measurement of the hysteresis loop

$$W_c = f\Delta\sigma\Delta\varepsilon_p \tag{3}$$

where $\Delta\varepsilon_p$ = plastic strain range, f = the fraction of the product of $\Delta\sigma\Delta\varepsilon_p$ actually traced out by the hysteresis loop gives

$$\Delta\varepsilon_p = \frac{W_{co}}{fC_1} d^{-(m-n)} \tag{4}$$

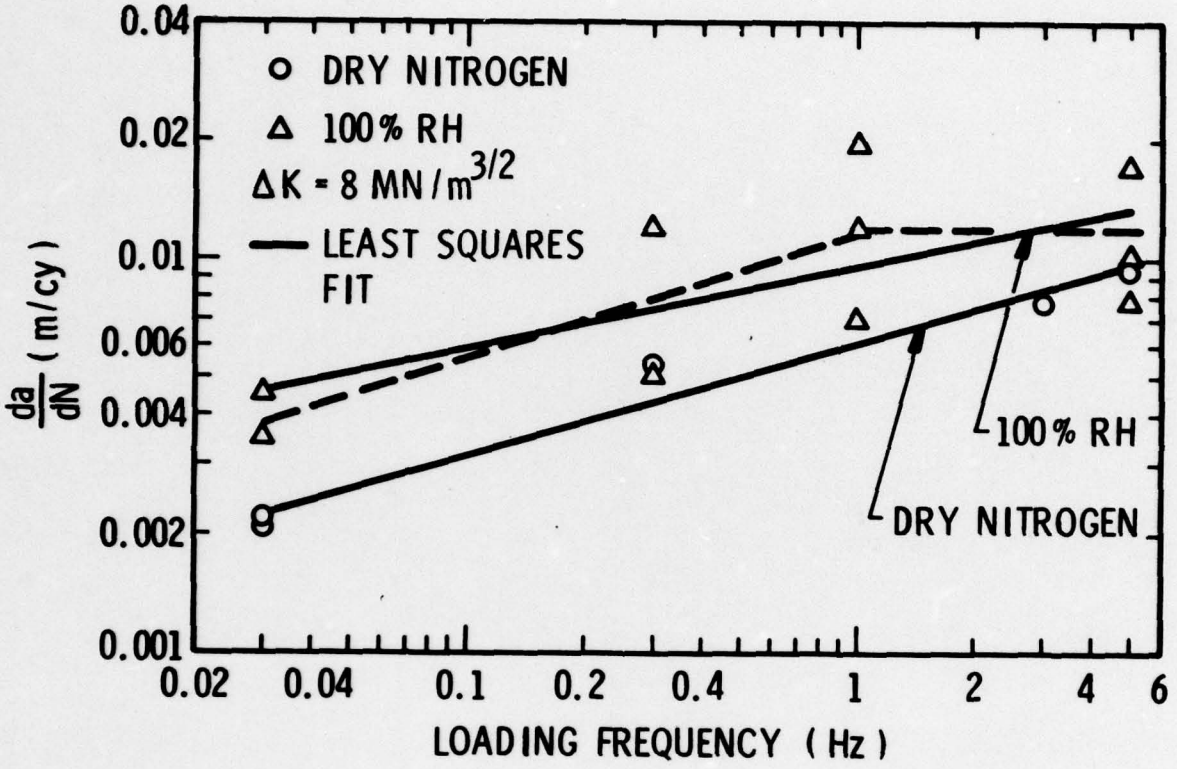

Figure 18. The effect of loading frequency on rate of crack propagation. The dotted line is an alternative explanation to the least squares fit.

which, using the experimentally derived values of the constants, and f = 0.7 gives

$$\Delta\varepsilon_p = 8.7 \times 10^{-3}\, d^{-0.738 \pm 0.1} \tag{5}$$

Similarly a cyclic stress-strain curve can be derived using these relations. The general form of this equation is[7]

$$\Delta\sigma = K'\sigma_y \left(\frac{\Delta\varepsilon_p}{2}\right)^N \tag{6}$$

where K′ is an experimentally determined constant, and N is a coefficient of work hardening.

Combining Eqs. (2) and (4) gives

$$\Delta\sigma = C_1 \left(2\,\frac{fC_1}{W_{co}}\,\frac{\Delta\varepsilon_p}{2}\right)^{\frac{n}{m-n}} \tag{7}$$

which is of the same form as Eq. (6).

Substituting values for the constants in Eq. (7) gives

$$\Delta\sigma = 12\,\sigma_y \left(\frac{\Delta\varepsilon_p}{2}\right)^{0.36 \pm 0.05} \tag{8}$$

The derived value of N is in good agreement with other results. Rice and Rosengren[8] concluded that for power law hardening materials, with work hardening coefficient N,

$$\sigma \propto r^{-\frac{N}{1+N}} \tag{9}$$

and

$$\varepsilon \propto r^{-\frac{1}{1+N}} \tag{10}$$

For the value of N derived in Eq. (8), these coefficients are:

$$\frac{N}{1+N}\ (\text{stress}) = 0.24$$

$$\frac{1}{1+N}\ (\text{strain}) = 0.76$$

For annealed iron, Landgraf[7] found N = 0.24 ± 0.04 which approximates the 0.36 ± 0.05 of Eq. (8). The stress range exponent of 0.262 (Eq. (2)) is very close to the theoretical value of 0.24, and the strain range coefficient of 0.74 ± 0.1 is also approximately equivalent to the 0.76

derived from power law hardening. The only serious inconsistency rises in the comparison of the derived value of K′ of Eq. (6), which differs by a factor of 3.5 from that experimentally found by Landgraf. In summary, the relationship between subgrain size and stress given in Eq. (2) appears to be well justified by other experimental data and by theoretical analysis which includes work hardening.

The derived stress range and strain range distributions, Eqs. (2) and (4), have the same functional dependence and roughly the same slopes as the analytical theory of Rice and Rosengren for a non-cyclicly loaded crack for distances several micrometers from the crack tip. Near the crack tip, however, the theoretical results predict stress and strain singularities, while the experimental results are bounded. The finite element work of Levy, et al,[9] also for a non-cyclicly loaded crack, conversely, does indicate a limiting stress at the crack tip of 3 σ_y, (for the non-strain hardening case) which is roughly comparable to the experimental value of 2.25 σ_y. The shape of plastic zone, discussed more completely in Ref. 1, is very similar to that determined by Levy, et al (their Fig. 4), except that their values of plastic zone size are about a factor of 3 larger than the measured subgrain forming region. Tracey[10] has also calculated the stress distribution for a non-cyclicly loaded crack using the finite element method, but for a work hardening material. For N = 0.3, Tracy obtains a maximum value of stress at the crack tip of 5 σ_y. All of the finite element analyses assume unbounded distributions of stress and strain given by Eqs. (9) and (10).

Strain Range Determination

Derivation of the strain range from subgrain size, Eq. (5), has several embedded assumptions, which can be examined by using the stereo-imaging technique. Subgrain formation is thought to be related to γ_{max}, so it is this quantity which was used to derive values of the constants in Eq. (11), which has the same form as Eq. (4):

$$\Delta\varepsilon_p = \frac{E}{(A + Br)^m} \qquad (11)$$

where m = .738 from Eq. (5) and B = 0.15[1]. Table I gives the derived constants in the equation, γ_{max}, and the extrapolated dimension of the subgrain forming region (r_1).

TABLE I

Environment	A	E	γ_{max}	$r_1(\gamma = 1\%)$ (μm)
Dry nitrogen	0.09	0.111	0.203	170
Wet air	0.53	0.078	0.124	104

The derived values of A (the subgrain dimension at the crack plane) agree well with those measured by channeling contrast, as do the extrapolated values of r_1. The derived value of E, however, differs from that determined in Eq. (5) by about a factor of 10.

In summary, the form of the equation for $\Delta\varepsilon_p$ derived from subgrain size measurements agrees very well with that derived from direct measurement of the crack tip plastic strain by stereoimaging. Subgrain size distribution derived using the latter technique also agrees well with the measured subgrain size distribution.

Summary and Conclusions

1. Preliminary results, as determined by a new technique for determining crack tip strains, indicates that

   The strain distribution near a fatigue crack is described well by function

   $$\Delta\varepsilon_p = \frac{E}{(A + Br)^m}$$

   where A is related to the subgrain size at the crack tip, B is the slope of the change in subgrain size with distance, r, from the crack tip, m = 0.74, and E is related to the maximum shear strain, γ_{max}, experienced by the material at the crack tip. This function is the same as determined previously from the subgrain distribution as observed by backscattered electron imaging.

2. The stress range distribution, as determined from subgrain size measurements, is consistant with the above result, and other results as well.

3. A water vapor environment lowers the strain range, $\Delta\varepsilon_p$, which material at the crack tip can support.

4. The lower strain range resulting from the presence of water vapor could be caused by a number of changes in material properties; which is actually the cause has not yet been determined. Hydrogen is thought to be the environmental specie which is responsible for the changes.

5. Crack growth rate is shown to be both loading frequency and environment sensitive; thus, to completely understand the effect of environment, it will be necessary to eliminate the changes due to loading rate.

6. Preliminary results indicate that the "clamping strain" for the crack tip in the unloaded state is decreased by the pressure of water vapor. The hysteresis in crack tip opening is similarly affected.

REFERENCES

1. D. L. Davidson and J. Lankford, ONR Interim Report, June 1977 - June 1978.

2. D. L. Davidson, SEM/1979/Vol. II, pp. 79-86.

3. D. R. Williams, D. L. Davidson and J. Lankford, "Fatigue Crack Tip Plastic Strains by the Stereoimaging Technique," 1979, submitted to Experimental Mechanics.

4. W. A. Nash, Strength of Materials, 2 ed., McGraw-Hill, New York, 1972, p. 321.

5. G. W. Simmons, P. S. Pao and R. P. Wei, Met. Trans. A, 9A, pp. 1147-1158 (1978).

6. H. Mughrabi, K. Herz, and X. Stark, Acta. Met., 24, p. 659 (1976).

7. R. W. Langraf, "Work Hardening in Tension and Fatigue," AIME, New York, 1977, p. 240.

8. J. R. Rice and G. F. Rosengren, J. Mech. Phys. Solids, 16, pp. 1-12 (1968).

9. N. Levy, P. V. Marcal, W. J. Ostergren and J. R. Rice, International Journal of Fracture Mechanics, 7, pp. 143-156 (1971).

10. D. M. Tracey, Journal of Materials Technology, 98, pp. 146-151 (1976).